JAAS

Journal of Analytical Atomic Spectrometry

www.rsc.org/jaas

Volume 28 | Number 10 | October 2013 | Pages 1533–1668

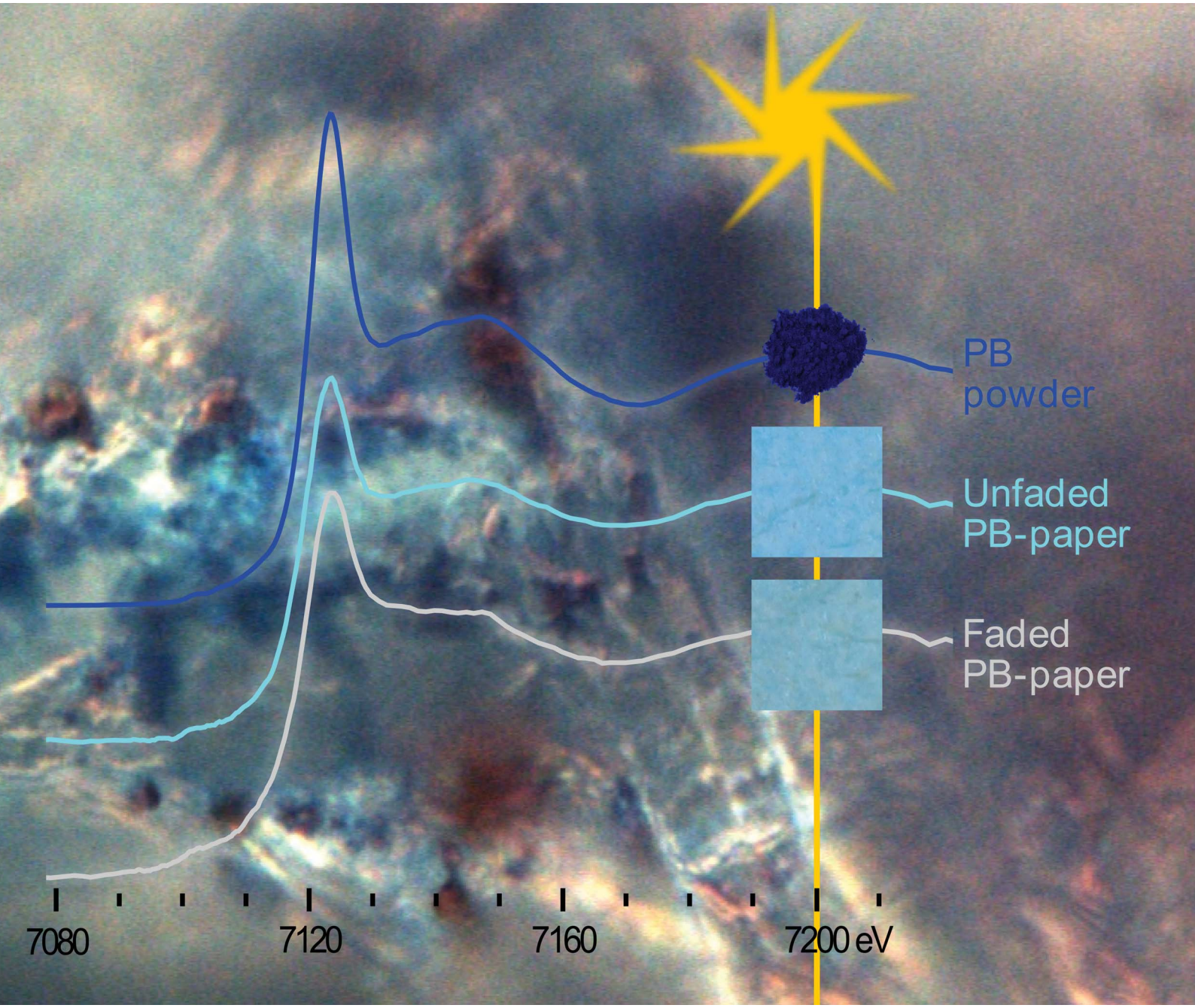

ISSN 0267-9477

RSC Publishing

PAPER

Claire Gervais *et al.*

Why does Prussian blue fade? Understanding the role(s) of the substrate

JAAS

RSC Publishing

PAPER

Why does Prussian blue fade? Understanding the role(s) of the substrate

Cite this: *J. Anal. At. Spectrom.*, 2013, **28**, 1600

Claire Gervais,†*[a] Marie-Angélique Languille,[b] Solenn Réguer,[c] Martine Gillet,[d] Sébastien Pelletier,[b] Chantal Garnier,[d] Edward P. Vicenzi[a] and Loïc Bertrand[bc]

Received 23rd January 2013
Accepted 5th August 2013

DOI: 10.1039/c3ja50025j

www.rsc.org/jaas

Prussian blue (PB) and its analogues are widely studied because of their interesting and promising magnetic and optical properties. The pigment Prussian blue, found in different types of artworks (paintings, watercolors and photographs), is also studied in the area of heritage science, where its capricious fading behavior under light or anoxia treatment poses problematic conservation issues. PB fading is due to the reduction of iron(III) to iron(II) and depends significantly on the artefact. This paper focuses on the roles of the substrate in affecting the PB structure and modifying the redox process. In particular, X-ray absorption experiments at the Fe K-edge of unfaded and faded PB–paper samples show that changes in the PB structure can happen by simple contact with the substrate, prior to the fading treatment. Spectrophotometric measurements on a series of model PB–paper samples further demonstrate the multiple influences of the substrate and show that not only its chemical composition but also its role as a dispersion and textured medium significantly alter the fading behavior of PB. A potential roadmap is proposed to rationally investigate the complex fading process of Prussian blue on a substrate.

1 Introduction

Prussian blue (PB, iron(III) hexacyanoferrate(II)) is a pigment widely used in Europe in the 18th and 19th centuries. Among famous objects containing Prussian blue are paintings from Watteau (1684–1721), Van Gogh (1853–1890) and Picasso (1881–1973), watercolors from Hokusai (1760–1849), and also precious testimonies of our history such as the world's second official postage stamp "Two Penny Blue", or one of the first types of color photographs, the trichromies of Louis Ducos du Hauron.[1] Artefacts composed of Prussian blue pose several challenges for conservation efforts, among which are their sensitivity to light or to anoxic treatment.[2–4] Under intense illumination or in a low-oxygen environment, PB undergoes discoloration. Keeping PB in the dark in ambient air reverses fading. However, it is still unclear whether the pigment fully recovers its original color or if an irreversible change in the structure and chemical state of PB occurs and to what extent.[1] Furthermore, the lightfastness of PB seems to be highly variable and contradictory fading behaviors have been reported in the literature.[2,3,5,6] This variability is still not understood and does not allow conservators to predict the light sensitivity of PB-containing artefacts and thus propose adequate conservation recommendations. We here investigate the physico-chemical process at the origin of PB fading in view of rationalizing the fading diversity observed in PB artefacts. For that purpose, we use model samples and focus on the substrate in which PB is embedded.

Prussian blue's structure exists in two forms, namely a cation-free form $Fe_4[Fe(CN)_6]_3 \cdot 12–14H_2O$ (PBI) and a cation-containing form $KFe[Fe(CN)_6] \cdot 3–5H_2O$ (PBS). The crystal structure of PBI can be described as a rock salt structure where $Fe^{II}(CN)_6$ and Fe^{III} alternate at the vertices of the cubes.[7,8] For charge balance, approximately 25% of the $Fe^{II}(CN)_6$ sites are vacant and filled with water molecules located at empty nitrogen sites and coordinated to Fe^{III}.[8] The amount of water molecules varies with the synthesis and environmental conditions. The crystal structure of PBS remains elusive. Based on powder diffraction measurements, Keggin and Miles described it as the same cubic structure as PBI, but without $Fe^{II}(CN)_6$ vacancy and with K^+ cations located in the octahedral interstitial sites.[9] This structure is still nowadays used for schematically describing powder PBS obtained by wet chemistry.[4]

[a]*Smithsonian Museum Conservation Institute, 4210 Silver Hill Road, Suitland, Maryland 20746, USA. E-mail: claire.gervais@bfh.ch*

[b]*IPANEMA, USR 3461 CNRS/MCC, Synchrotron SOLEIL, BP48 Saint-Aubin, F-91192 Gif-sur-Yvette, France*

[c]*Synchrotron SOLEIL, BP48 Saint-Aubin, F-91192 Gif-sur-Yvette, France*

[d]*Muséum national d'histoire naturelle CRCC, USR3224 CNRS/MCC, CP21, 36 rue Geoffroy-Saint-Hilaire, 75005 Paris, France*

† Present address: Bern University of the Arts, Fellerstrasse 11, CH-3027 Bern, Switzerland, E-mail: claire.gervais@bfh.ch

Prussian blue's color is due to intervalence charge transfer between low-spin Fe^{II} and high-spin Fe^{III} centers, leading to absorption around 640 nm,[10]

$$\{Fe^{III} - C\equiv N - Fe^{II}\} \overset{h\nu}{\rightleftharpoons} \{Fe^{II} - C\equiv N - Fe^{III}\}^{\star}, \quad (1)$$

where ★ denotes an excited state. Thus, the color depends on the amount of Fe^{II}–C≡N–Fe^{III} units and will be influenced by any disturbance in this pattern, such as the amount of vacancies[11] or the presence of coordinated water molecules within vacancies.[12]

Prussian blue's discoloration is due to the reduction of Fe^{III} to Fe^{II} ions, leading to the formation of Fe^{II}–C≡N–Fe^{II} units, where charge transfer in eqn (1) does not happen anymore. This redox process has been particularly investigated for electrochemically synthesized PB (ESPB) films due to their interesting applications in the field of biosensors and ion detection.[13–15] It can schematically be summarized as:

$$KFe^{III}[Fe^{II}(CN)_6] + K^+ + e^- \rightleftharpoons K_2Fe^{II}[Fe^{II}(CN)_6], \quad (2)$$

although the process is more complex, with different participation of the Fe^{III} sites, depending on whether they are in the vicinity of Fe^{II} vacancies or fully surrounded by $Fe^{II}(CN)_6$ clusters.[15] What stands out is that the redox properties of ESPB depend on the overall ability of cations to enter and exit the structure upon reduction and oxidation, respectively.[16]

Light fading of Prussian blue in cultural artefacts is a process identical to that in eqn (2). Under UV-visible light, Prussian blue artefacts undergo a reduction of Fe^{III} leading to progressive discoloration.[4,17,18] The reaction reverses in the dark in ambient atmosphere, with slow re-oxidation of the bleached Prussian blue and recovering of the blue color. The main difference with ESPB lies however in the source of electrons and cations necessary for the reaction in eqn (2) to take place. In ESPB, electrons are provided by artificial voltage and cations are provided by the electrolytic solution. In PB artefacts, the identification of the electron-donor and the source of cations remains an open question. As the lightfastness of pure PB powder is considered to be excellent by the manufacturers and has been confirmed by ourselves for in-house synthesized PB, the source of cations and electrons has to be external to the pure powder and does not come from an internal rearrangement of the structure.

The presence of a substrate needs therefore to be considered as an external reservoir. Recent studies on iron ink–paper,[19] dye–paper[20] and Prussian blue–paper systems have indeed shown that this correlation cannot be neglected.[17,18] Typically, the substrate may participate in the PB reduction process in three different and non-self-excluding ways:

(i) The main molecular components from the substrate itself may be electron-donors and thus participate in the reduction process of Prussian blue. This could be the case for paper and plant textiles, typical substrates of PB artefacts. For instance, as suggested in earlier studies,[18] the chemical composition of paper (cellulose *vs.* lignocellulose) might have an impact on the kinetics of PB fading.

(ii) The substrate can act as a carrier of impurities that may be involved in the reduction process. This is likely to be the case for cyanotypes, an early photographic contrast-printing process based on Prussian blue, where impurities derived from the sensitizer (*e.g.* oxalate or citrate ions) are present in the paper substrate.[4,17] Similarly, while Prussian blue is usually stable in paintings, its lightfastness is dramatically decreased in mixtures with lead white pigments.[5] As proposed recently, a possible explanation is the reduction of Fe^{III} at the surface of Prussian blue triggered by the near vicinity of basic lead compounds.[21]

(iii) The distribution of PB within the substrate almost certainly plays a role in the color and color change as well. The particle size and particle distribution are known to influence the color by an interplay between absorption and scattering of light.[22] Besides, the distribution of the pigment within the substrate matrix is obviously another factor to be considered with regard to the amount of light exposure.[23,24] Finally, the porosity and permeability characteristics of the substrate may well play a role by controlling the access of PB to water and oxygen contents.

The goal of this paper is to probe the potential roles (i)–(iii) of the substrate in the reduction process of PB and propose potential routes for further investigation. To that aim, a methodology based on the analysis of artificially faded model PB artefacts was developed. PB–paper model samples composed of the same PBS powder synthesized in-house and artificially faded were investigated by means of X-ray Absorption Near Edge Structure spectroscopy (XANES), spectrophotometry, Scanning Electron Microscopy (SEM) and Raman spectroscopy. Two types of paper were chosen for their different stability under light to investigate the correlation between light-sensitivity of the substrate and PB fading (effect (i)). The role of the substrate in supplying cations necessary for the reduction of PB to occur (effect (ii)) was studied by adding KCl to the PB–paper system and monitoring its fading behavior by means of spectrophotometry. The impact of PB spatial distribution within the substrate (effect (iii)) was studied by comparing the fading behavior of PB–paper systems with different PB concentrations and by probing the spatial and chemical heterogeneities of PB within the sample. Finally, the diversity and complexity of factors influencing the fading behavior of such a rather simple type of system were put into the context of the fading of PB artefacts. For that purpose, a series of different PB model artefacts were prepared and their fading behavior was monitored by XANES and colorimetry. A potential roadmap is proposed to study more systematically the various structural and chemical factors intrinsic to the PB–substrate systems, which might play a role in the observed fading diversity.

2 Experimental

Synthesis and sample preparation

Synthesis of Prussian blue (PBS). An equivolume of potassium hexacyanoferrate solution ($K_4Fe^{II}CN_6$, 0.2 M) is added dropwise to a stirred solution of iron sulfate ($Fe^{II}(SO_4)\cdot 5H_2O$, 0.1 M). The precipitate was filtered, washed with deionized water, dried at 60 °C and manually ground.

Paper samples (PBS–*Whatman* and PBS–*Step3*). The two chosen papers are those used in ref. 18, that is *Whatman*, composed of 100% cotton cellulose fibres and *Step3* a

lignocellulosic paper (75% round wood pulp + 25% soft wood cellulose) containing fillers (kaolin at 20%) and sizing (alum, rosin).[25] A colloidal solution of synthesized PBS was prepared (25 mg in 1 mL of deionised water) and deposited on *Whatman* and *Step3* papers by brushing (Fig. 1 and 2). Weight measurements confirmed the deposition of similar amounts of PBS on both papers. To study the effect of cations as shown in Fig. 5, a colloidal solution of PBS was prepared by adding PBS in a 1 M KCl solution instead of water. For colorimetry studies (Fig. 4 and 6), small strips of papers were immersed into the colloidal solutions for 5 seconds and then dried at room temperature. The initial sample (named as d0) was prepared with a concentration of 25 mg PBS in 1 mL of deionised water. Dilutions were then prepared with deionized water to obtain relative concentrations of 1/2, 1/3, 1/4, 1/9, 1/20, and 1/30, named as d1, d2, d3, d4, d5 and d6 respectively.

Textile samples (cotton and silk). Cotton and silk textiles were dyed according to a modern version[2] of Napier's recipe.[26] The tissues were soaked for 30 minutes in a solution of iron nitrate ($Fe^{III}(NO_3)_3 \cdot 9H_2O$, 7.65 g in 1 L water). After wringing, they were immersed in a solution of 7.56 g potassium ferrocyanide ($K_4Fe^{II}CN_6$) and 1.9 mL of sulfuric acid (H_2SO_4, 0.4 M) in 1 L of water. This two-step immersion procedure was then repeated before soaking the clothes for 2 or 3 minutes in a solution of aluminum sulphate (0.95 g in 1 L of water) in order to fix the dye. Finally, clothes were rinsed in water and dried at room temperature.

Ducos du Hauron samples (DDH). These samples relate to the first color prints introduced in 1868 by Louis Ducos du Hauron,[1] which are obtained by superposition of three colored gelatin layers respectively in blue, red and yellow on a paper base, the blue layer being colored with Prussian blue. Samples studied here refer only to the PB blue gelatin layer and are those prepared by Lavédrine *et al.*,[1] according to Ducos du Hauron's recipe from 1870.

Cyanotype samples (cyano). Cyanotypes were prepared with vélin paper according to Herschel's recipe, which consists of an equal proportion mixing of an aqueous solution of ammonium iron(III) citrate (20 g in 100 mL of water) and potassium ferricyanide ($K_3Fe^{III}CN_6$, 8 g in 100 mL of water). The cyanotype is then revealed by exposing it to natural light and then was briefly rinsed to stop the process.

Paint samples (paint). Paintings consist of linen canvas covered with a ground layer composed of a 7% solution of rabbit glue and hydrated calcium sulfate. PBS was ground in linseed oil and applied on top of the ground layer.

Fading treatment. Samples were placed into a light weathering chamber equipped with a metal halide lamp (2500 W Hydrargyrum Medium-arc Iodide (HMI) lamp) and a window glass filter that removed UV radiation below 325 nm. Light aging was performed at $T = 25$ °C and 50% RH. We attempted to mimic alteration during 3400 museum hours (based on a 50 lux exposure) by a fading treatment of about 170 K lux at the surface of the samples and an irradiance of about 1200 W m^{-2}. Three series of samples were prepared and underwent the fading treatment for five days. For each sample, a part was hidden from the light as a reference. The color was measured before and immediately after light exposure.

Characterisation methods

Scanning electron microscopy. SEM images were recorded on a SEM-FEG able to work under a controlled atmosphere (ZEISS Supra 55VP) equipped with a 30 mm^2 SDD detector (Bruker). Secondary electron (SE-SEM) images were saved at low voltages to avoid charge effects. Higher voltages under $p(N_2) =$ 0.1 mbar were used for backscattered electron (BSE-SEM) images and EDX mappings, especially to excite the Fe-Kα transition.

X-ray diffraction. X-ray diffraction experiments were performed on the CRISTAL beamline at SOLEIL synchrotron. The wavelength of 0.7931 Å ($E = 15634$ eV) was extracted from the undulatory beam by means of a double crystal Si(111) monochromator. The powder was introduced into a rotating quartz capillary of 700 μm in diameter, mounted on a two circles diffractometer equipped with a 21 crystals multi-analyser. It took less than 30 min in continuous scanning mode to collect high angular resolution diagrams. The diagram is obtained by addition of the 21 channel data. LaB_6 and NAC were both used as standards to calibrate the instrumental broadening and potential shift in the location of the diffraction peaks. We tested the stability of the powder under the beam by recording several successive scans on the same area. After 10 scans, no difference in the XRD diagram was observed.

Spectrophotometry. Color measurements of the samples were performed with a sphere spectrophotometer X-Rite SP64, which provides reflectance spectra (resolution 10 nm) and L^* a^* b^* color parameters of the sample with L^*: lightness, a^*: red-greenness, and b^*: yellow-blueness. The measured area was 10 mm in diameter. The total color difference ΔE was calculated using the CIE 1976 L^* a^* b^* equation for the 10° standard observer and the standard illuminant D65.[10]

X-ray absorption spectroscopy. XANES spectra were collected at the DiffAbs beamline of SOLEIL synchrotron . The energy scans were measured from 7050 eV to 7300 eV with 0.5 eV energy resolution, using the Si(111) double crystal monochromator and a macrobeam spot size of about 300 μm^2. The incident beam intensity and transmitted signal were measured using Si photodiodes, while the fluorescence signal was monitored using a silicon drift detector. Calibration of the XANES spectra was performed with reference to the inflexion point of a Fe foil at 7112 eV. XANES spectra were processed with the Athena software (Iffefit 1.2.9 program suite).[27] The pre-edge range background was removed by subtracting a Victoreen function and the absorption background was removed using a cubic spline in a normalisation range between 30 and 270 eV after the edge. All XANES spectra presented here are the average of two normalized spectra obtained successively at the same location. No beam damage could be detected (*i.e.* no change of the spectrum between the two successive spectra and no visible alteration of the sample).

Raman spectroscopy. Raman spectra were recorded using a Thermo Scientific DXR Raman microscope equipped with a 532 nm diode laser. The backscattered light was dispersed by a 900 L mm^{-1} grating and the Raman signal was detected with a Peltier cooled charge-coupled device. The spectral resolution

was in the 5.5–8.3 cm^{-1} range. A 100× objective (numerical aperture of 0.9) was used, *i.e.* the estimated laser spot is of approximately 700 nm in diameter. Each spectrum was collected for 5 min, with a power of 500 μW without any observable laser-induced alteration of the samples.

3 Results and discussion

3.1 Characterisation of PBS

Soluble Prussian blue (PBS) was synthesized by wet chemistry according to the procedure reported in ref. 28. Elemental analysis by two methods (EDX and atomic emission spectroscopy) confirmed the synthesis of soluble Prussian blue KFe $[Fe(CN)_6]\cdot xH_2O$ with a Fe : K ratio of 2 : 1. The exact stoichiometry of water could not be precisely determined. Traces of sulfur were detected by EDX (normalized percentage of 1% w/t) and likely come from the starting product iron sulfate. The structural purity of the powder was checked by synchrotron X-ray diffraction (the signal-to-noise ratio obtained on a laboratory X-ray diffractometer was insufficient for that task). Fig. 1 shows the room-temperature X-ray diffraction pattern, with its best fit (Rwp: 2.33%) by the LeBail pattern decomposition technique[29] implemented in GSAS.[30] The XRD pattern could be indexed in face-cubic symmetry (space group $Fm\bar{3}m$, $a = 10.198$ Å), in agreement with the literature.[7,9] The crystallite size was calculated based on the Scherrer formula and estimated to be around 140 nm. Best profile refinement was achieved by taking into account microstrain effects (lattice defects), also responsible for peak broadening. Therefore, although both crystallite size and strain contributions can be theoretically distinguished, this estimate value of 140 nm needs to be taken with caution. Scanning electron microscopy reveals a PBS powder composed of aggregates with undefined shapes and variable sizes (Fig. 1, inset). Distinct nanoparticles are however visible, of a size comparable to the averaged crystallite size estimated by XRD (white circles). Both estimated crystallite and particle sizes fall into the nanoscale regime. This result is not surprising, considering the low solubility of PBS in water leading to its very fast precipitation upon synthesis. One direct consequence of this nanosize is that PBS powder has a large specific surface area and is therefore likely to be very sensitive to its environment.

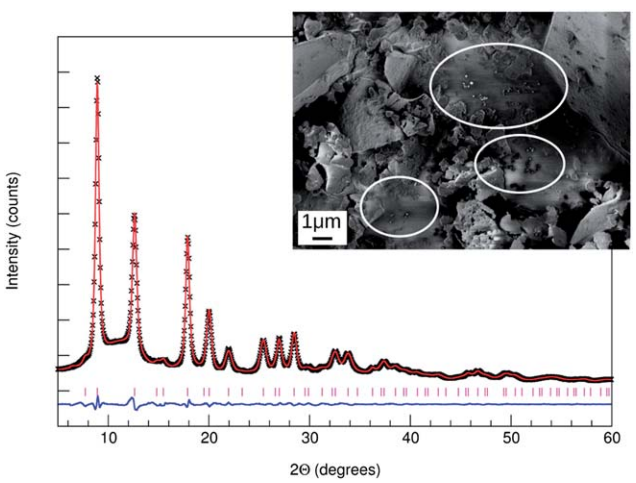

Fig. 1 Diffraction pattern of PBS at 293.0 K, $\lambda = 0.7931$ Å (cross), its LeBail fit (line) and residues (vertical bars mark the Bragg reflection). Inset: SE-SEM image of PBS powder (working distance: 2 mm; accelerating voltage: 0.5 kV, $p = 5 \times 10^{-7}$ mbar). Circles indicate regions where distinct nanoparticles may be observed.

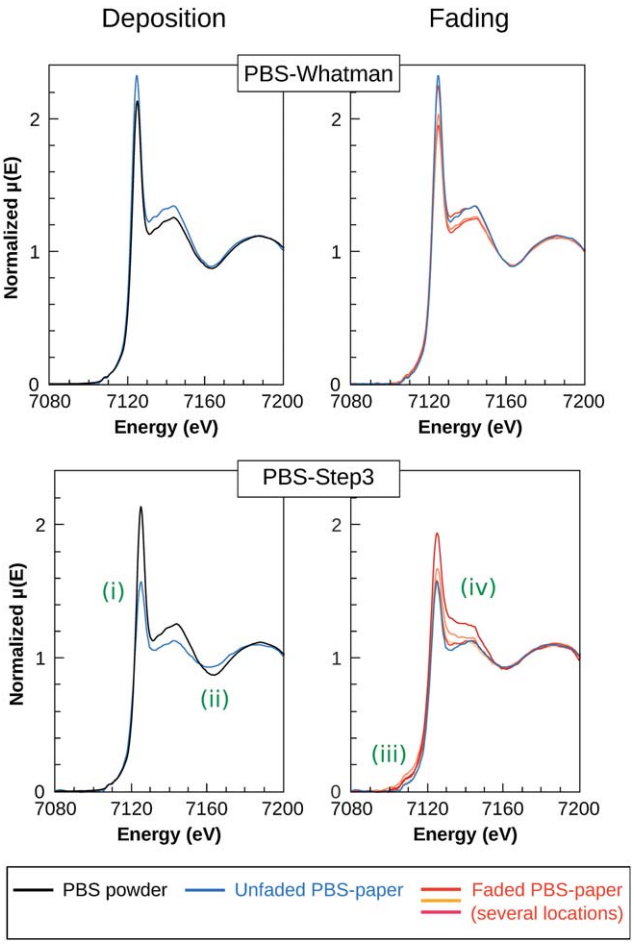

Fig. 2 XANES spectra of PBS powder (black) and PBS–paper samples before (blue) and after fading (red-orange). Due to heterogeneity observed in the faded PBS–paper samples, measurements were performed at three to five different locations of each sample (red-orange curves). For PBS–*Step3* samples, structural variations are observed both before and after light exposure and occur in four regions of the spectra denoted (i)–(iv).

3.2 The substrate influences both the structure and redox properties of PB

In order to focus on the substrate and remove any influence due to the PB crystal structure, we investigated PBS–*Whatman* and PBS–*Step3* paper model samples, both prepared with the same PBS powder as described above. As explained in previous work,[18] the two papers were chosen for their different stabilities under light: *Whatman* paper is pH-neutral cellulosic paper often used as suitable paper for conservation treatments. In contrast, *Step3* paper is light-sensitive ligno-cellulosic paper chosen for its high acidity (pH = 5.4) and its ability to readily oxidize.[25] Iron speciation and the color of PBS–*Whatman* and PBS–*Step3*

samples were analyzed before and after fading by means of XANES at the Fe K-edge and spectrophotometry, respectively. Other techniques revealed to be not very informative. For instance, extended X-ray absorption fine structure spectra exhibited only weak oscillations due to strong multiple scattering often found in cyano-bridged organometallic compounds.[31] Besides, X-ray diffraction data proved to be ineffective due to the presence of a large amorphous part of the cellulosic substrate and an overlap between the diffraction peaks of PB and the crystalline part of cellulose.

Structural changes of the environment of iron atoms monitored by XANES at the Fe K-edge are significantly different between the two PBS–paper samples (Fig. 2). Unfaded PBS–*Whatman* features similar spectra to PBS powder and only a slight loss of intensity at the absorption edge is noticed after fading. In contrast, for PBS–*Step3* systems, pronounced changes happen both upon deposition of the PBS powder on the paper and after fading. Changes may be classified into four regions numbered (i)–(iv) in Fig. 2.

After deposition of PBS powder on *Step3* paper, the XANES spectrum of the PBS–*Step3* sample exhibits broadening of the absorption edge (region (i)). It manifests by a lowering in the intensity of the maximum of the derivatives of the XANES spectra (Fig. 3) and is associated with a slight shift (below 1 eV) of the edge towards lower energies. The broadening might be correlated with the presence of more irregular or disordered Fe sites,[32] while the shift in energy indicates a slight reduction of Prussian blue. Both features do not seem to be enhanced by light exposure. The unfaded PBS–*Step3* sample also features a shift of ~2.5 eV of the position of the 1st oscillation compared to PBS powder (region (ii)). It may be indicative of an increase of the distance to neighbors associated with a geometrical distortion of the Fe^{II}–C≡N–Fe^{III} units.

After fading, the XANES spectrum of PBS–*Step3* exhibits additionally a more intense pre-edge peak at 7108 eV (region (iii)). It could be attributed to a change in the oxidation state from Fe^{III} to Fe^{II}, a deviation from the perfect octahedral coordination state of iron clusters or an elongation/contraction of the iron–CN ligand distance.[33] Unfortunately, the pre-peak signal was too noisy to be further processed. Fading also induces a significant change of the slope in the post-peak region (range 7125–7162 eV, region (iv)). In cyanoferrates, this region is governed by very large multiple-scattering effects due to the presence of the C≡N pattern.[34] A change in this region of the spectrum thus involves a modification of the Fe^{II}–C≡N–Fe^{III} units, either geometrically or in terms of oxidation state. It is worth noting that the change of slope is observed in all five XANES measurements performed on the faded sample at different locations (red-orange curves, Fig. 2), but the degree to which the slope changes varies significantly from point to point. It thus indicates that the modification in the spectral region (iv) is present all over the sample but with some spatial heterogeneity.

Reflectance curves of PBS–paper samples are presented in Fig. 4. Before light exposure, PBS–*Whatman* and PBS–*Step3* samples exhibit a different spectrum at the position of the maximum of reflectance (450 nm and 465 nm respectively). However, this difference between the two unfaded PBS–paper samples cannot be straightforwardly related to that observed in XANES spectra, as the blue-green region (400–550 nm) is dominated by interband transitions of the paper (black curves).

After fading, the change of reflectance curves differs also for PBS–*Whatman* and PBS–*Step3* samples, with ΔE values of 3.8 and 13.0, respectively. The distinction takes place in the range of 400–550 nm, where reflectance values of both PBS–*Step3* and *Step3* paper alone are significantly decreased (red and gray curves, Fig. 4, right). This may be attributed to the phenomenon of "paper yellowing", a result of the oxidation of the lignin present in *Step3* paper, which releases chromophores absorbing in the blue-green region.[35] In the wavelength domain of 550–700 nm, absorption by Fe^{II}–C≡N–Fe^{III} occurs and gives its color to

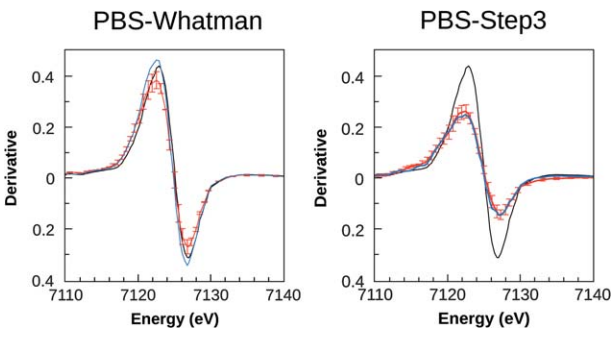

Fig. 3 Derivatives of the XANES absorption spectra illustrating the broadening of the absorption edge for PBS–*Whatman* and PBS–*Step3* samples. Powder (black) and PBS–paper samples before (blue) and after fading (red). Errors bars correspond to standard deviations on 4 and 5 measurements for PBS–*Whatman* and PBS–*Step3* respectively.

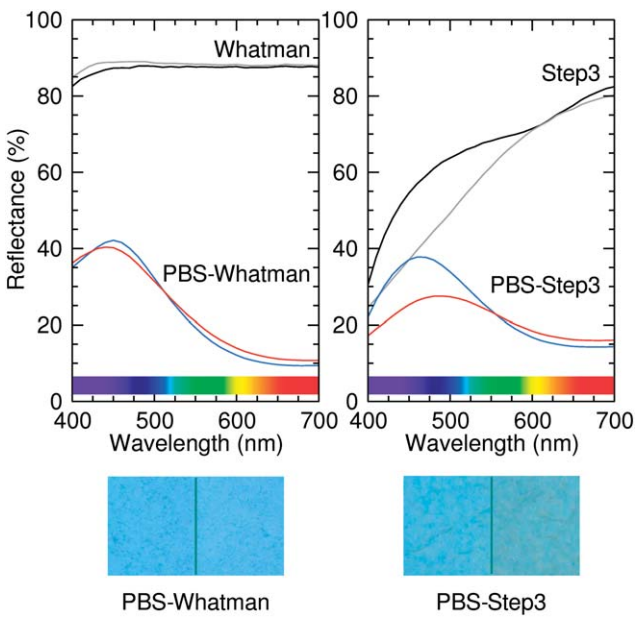

Fig. 4 Reflectance curves of PBS–paper samples before (blue) and after fading (red). For reference, reflectances curves of papers alone before (black) and after fading (gray) are indicated. Bottom: optical photographs of the unfaded and faded samples (respectively left and right parts of the photographs).

Prussian blue (eqn (1)). The photoreduction of Prussian blue, leading to non-absorbing Fe^{II}–C≡N–Fe^{II} blocks, would thus impact principally this region and lead to a higher reflectance. Interestingly, the fact that both samples behave similarly in this region might thus indicate that Prussian blue reduction happens to the same extent in both samples. With respect to geometrical distortions of the crystal lattice of Prussian blue, they would lead to band broadening or shifting.[36] The fact that they are not visible does not indicate their absence, as the low spectral resolution (10 nm) associated with the overlap of the intervalence charge transfer in Prussian blue with paper absorption bands might hide such spectral features.[24]

Clearly, all these variations upon deposition and fading need to be further investigated to understand the exact types of structural modifications taking place during the fading process. However, considering the ability of Prussian blue and its analogues to accommodate ions within the lattice[36] and the presence of a mobile and disordered water network,[37] one may surmise that the geometrical distortions and other structural changes observed in PBS are likely due to reorganisation of the water network and/or migration of ions within the structure, either in tetrahedral sites or in iron vacancies.

Considering the role of the substrate, results shown here allow us to draw some important conclusions concerning the structural and redox properties of Prussian blue on the two types of paper.

First, compared to the reference PBS powder, structural changes happen on PBS–*Step3* before fading. As observed in XANES spectra, they likely involve geometrical distortions of the Prussian blue lattice associated with a slight reduction of PB. That is, the structure of the pigment has already been modified by simple "contact" with the *Step3* paper. A reaction occurred spontaneously between the pigment and the *Step3* paper that did not require visible light energy for activation. Several components in *Step3* paper could play such a catalytic role. For instance lignin is known to readily oxidize[38] and adsorption of chromium ions on a lignocellulosic substrate resulted in spontaneous reduction of the metal and oxidation of lignin.[39] Also, alum (aluminium double salts) is responsible for the low pH of the paper (pH = 5) and might have induced a structural change in PB. In contrast, no difference is observed between PBS–*Whatman* and PBS powder, a result showing that *Whatman* paper (composed of pure cellulose) is neutral with respect to the pigment in the frame of the experiment and does not induce spontaneous modification of its structure.

Second, changes of the PBS structure upon fading are not of the same nature on both types of paper, as exemplified by the variation in XANES spectra of the post-edge region occurring in PBS–*Step3* but not in PBS–*Whatman*. As just stated, the structure of PBS differs on both papers before fading (since *Step3* spontaneously modifies it) and this may be sufficient to explain the different fading behaviors. However, UV-vis reflectance spectra clearly show a higher degradation of *Step3* paper compared to *Whatman*, a process which in turn may influence the photoreduction of Prussian blue. As a comparison, acidity, such as that of *Step3*, was shown to impact the redox process of ESPB films by allowing hydrated proton transfer between the solution and Prussian blue.[37] Also, lignin present in *Step3* might be involved in the redox process by playing a role as a radical scavenger.[18,40]

In summary, these results indicate that the type of substrate has a major impact on both the structure and fading process of Prussian blue and that any study on light sensitivity of PB artefacts should take it explicitly into account. While it is shown that *Step3* paper has more influence on PB fading than *Whatman*, the reasons behind this have not been found yet. As stated in the former paragraphs and in previous work,[18] several hypotheses are plausible, such as the presence of lignin, acidity or the different distribution of PB within paper fibers. It seems therefore that the PBS–*Step3* system is still too complex if the goal is to rationalize, one by one, the various roles of the substrate. We have thus pursued our investigation by concentrating on the PBS–*Whatman* system, which is composed of two main components only (PBS and cellulose).

3.3 What are the roles of the substrate in the PB reduction process?

Although the importance of the various roles of the substrate cannot be estimated at this stage of the study, we have focused here on three properties of the substrate which seem to significantly influence PB fading: its role as a cation reservoir, as a dispersion medium and as a textured medium.

3.3.1 The substrate as a cation reservoir. According to eqn (2), cations are necessary to ensure electroneutrality of the reduced PBS. The PBS compound contains potassium (and possibly sulfur coming from the synthesis). However, PBS powder alone (*i.e.* without substrate) does not fade. This implies that we must look at the cations brought by the substrate. In Fig. 5, the influence of potassium on the fading process was tested by monitoring color changes of PBS–*Whatman* systems enriched in KCl.

The combined presence of KCl and light leads to a strong decrease of the absorption intensity in the 550–700 nm region (red curve). As *Whatman* paper enriched in KCl does not change upon fading (and KCl does not absorb in this region), this result indicates that the photoreduction process has been enhanced by addition of KCl. Several explanations can be advanced: first,

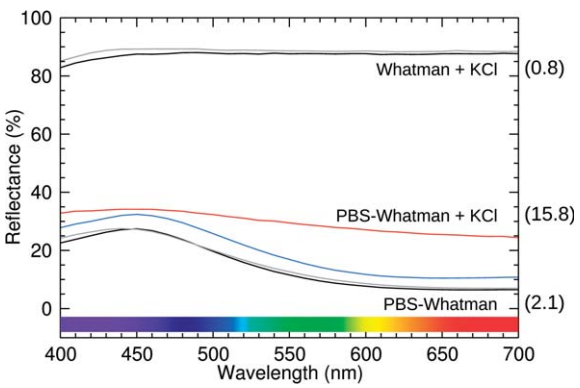

Fig. 5 Reflectance curves before (blue) and after fading (red) of PBS–*Whatman* systems enriched in KCl. Values in brackets refer to Δ*E* values. Control reflectances curves before and after fading of *Whatman* paper enriched in KCl and PBS–*Whatman* without KCl (sample d1) are indicated in black and gray, respectively.

migration of K^+ cations within the PB structure could take place to maintain electroneutrality upon reduction of Fe^{III} ions. This migration phenomenon has been well established in voltammetric cycles of ESPB.[16] Second, KCl is hygroscopic and its presence is likely to change the humidity content, both within the substrate and within the PB crystalline network. Concerning PB, water is known to influence the redox process in ESPB. Indeed, the ionic compensation following the change in the ratio of Fe^{III} : Fe^{II} may be given by electrolytes within the solution (*e.g.* K^+) but may also be obtained by changes in the composition (H^+/H_3O^+)[41] or in the amount[42] of coordinated water molecules in the PB crystalline network. Concerning the substrate, an increase of moisture may alter the stability of the cellulose[43] and hence participate indirectly in the redox process. XANES at the Fe K-edge and XRD on aliquots of samples shown in Fig. 5 are currently planned and should allow to better understand the influence of KCl on PB fading.

3.3.2 The substrate as a dispersion medium. The influence of the concentration of PB on fading is shown in Fig. 6. Diluted samples exhibit higher photoreduction of Prussian blue according to an exponential law between ΔE and relative PB concentration. This trend differs from the results of the impact of water dilution on the fading of PB watercolors (PB + gum arabic)[44] but has been verified by two independent sets of measurements on our systems and is also observed for PBS–*Step3* systems. This result shows the difficulty to compare PB fading for different substrates and highlights the need to use model samples with similar concentrations, *i.e.* with an approximately similar percentage of reflectance in the region of 550–700 nm, when comparing fading behaviors and color measurements.

3.3.3 The substrate as a textured medium. Finally, even in a given sample, the distribution of Prussian blue within a textured substrate such as paper leads to spatial and compositional heterogeneities.[45] SEM images of PBS–*Whatman* show a non-homogeneous distribution of PBS in the paper. The largest part of PBS is present in the form of a cracked crust located within and on top of the fibers. Its characteristics are similar to the PBS powder. However, microparticles with well defined shapes are also visible. This raises the question whether part of PBS did change upon deposition on the substrate. Indeed, the deposition step implied to put again PBS in solution. PBS is insoluble in water but forms submicroparticles (colloid) that could serve as nuclei for further growth once on the substrate. Raman spectroscopy performed on a PB particle and within a blue fiber shows a difference in the ^1A_g C≡N stretching vibration band at around 2150 cm^{-1} characteristic of PB.[46] The weak band around 2090 cm^{-1} corresponds to the E_g mode of the C≡N stretching vibration and does not seem to differ between the two types of PBS. Finally, the peak around 2120 cm^{-1} present in one of the spectra of PB particles could not be assigned but has been assigned to Prussian blue in ref. 47. This bimodal distribution of the particle size and location has thus a direct impact on the PB structure which is heterogeneous *at this scale*. Note also the chemical heterogeneity of the cellulosic fibers, which exhibit a non-uniform luminescence in optical photographs (Fig. 7). It emphasizes the fact that a medium such as paper, textured and chemically heterogeneous, obviously leads to more than a simple dispersion of the pigment. It interacts chemically and topologically with the pigment to form ultimately a complex material with paper–pigment interfaces varying in the area, chemical and structural type.

Owing to this multiple heterogeneity, it is particularly important to adapt the scale of the measurement to the property investigated, gather measurements at all the characteristic scales of the material[48] and be especially careful when comparing and correlating measurements obtained at different scales and information depths, such as Raman (estimated spot of 700 nm), XAS (averaging PB over a surface of 300 μm^2) or colorimetry (surface of 80 mm^2).

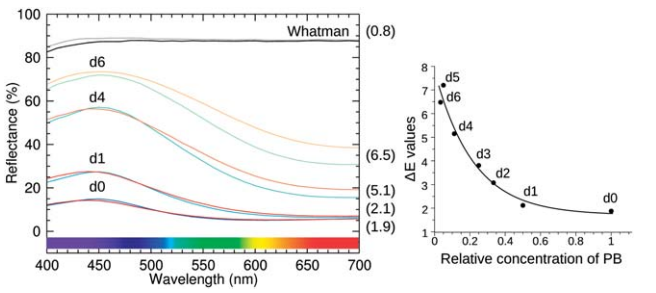

Fig. 6 Left: reflectance curves of PBS–*Whatman* paper systems at different PB concentrations, before (blue shades) and after fading (red shades). Values in brackets refer to ΔE values. For reference, the reflectance curve of *Whatman* alone before (black) and after fading (gray) is indicated. Right: relative PB concentration *vs.* ΔE, showing the entire relative concentration series [d0–d6]. Data could be fitted with an exponential law of the kind $a + \exp^{(-x/b)}$ (plain line).

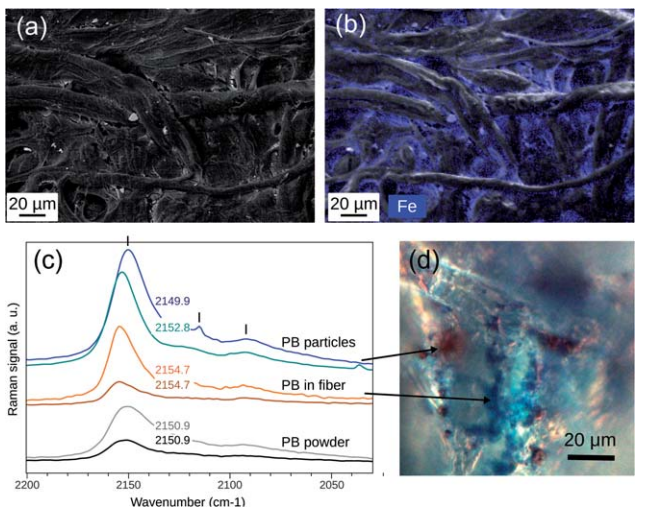

Fig. 7 Illustration of the microscale heterogeneity of Prussian blue in the morphology and structure. (a) BSE-SEM image of PBS–*Whatman* (working distance: 6.5 mm; accelerating voltage: 12 kV and $p(N_2) = 0.1$ mbar). (b) BSE-SEM image with Fe-Kα EDX mapping (300 px × 225 px). (c) Raman spectra of PBS powder and in PBS–*Whatman*. Vertical bars mark the three peaks attributed to PB and values indicate peak maxima corresponding to the ^1A_g mode of the σ(CN) stretching vibration band. (d) Brightfield optical micrograph of the PBS–*Whatman* sample, showing the presence of PBS particles (brown) and blue colored cellulosic fibers.

Table 1 Left: basic sample description showing the diversity of the model PB artefacts investigated. Major components and impurities in the samples are given based on the knowledge about the substrate and/or about the sample preparation procedure. Right: color changes (ΔE values) induced by a 5 day light exposure

Sample	Synthesis[a]	Substrate	Major components	Expected[b] impurities/additives
DDH	*in-situ*	Gelatin	Peptides/proteins	Yes
Paint	PBS	Oil	Fatty acids	No
Silk	*in-situ*	Textile	Proteins	Yes (sp[c])
PBS–*Step3*	PBS	Paper	Cellulose/lignin	Yes (fs[c])
Cotton	*in-situ*	Textile	Cellulose	Yes (sp[c])
Cyano	*in-situ*	Paper	Cellulose	Yes (sp[c])
PBS–*Whatman*	PBS	Paper	Cellulose	No
PBS	PBS	—	—	No

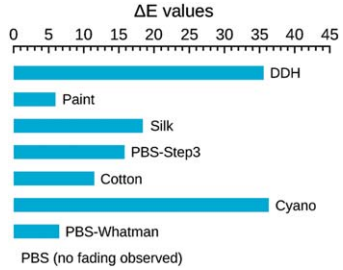

[a] Synthesis realized *in-situ* or *ex-situ* (powder PBS). [b] Expected to be present beside the major components of the substrate. [c] sp: starting products from synthesis; fs: fillers and sizing.

3.4 Fading behavior of model PB artefacts: a variability confirmed

Results presented so far have shown that even in "simple" PB–substrate systems, complex correlations between multiple factors influence the fading behavior of Prussian blue. This complexity should obviously be also considered for real PB artefacts, where additional chemical or spatial heterogeneities occur.[48] Table 1 presents a series of PB model artefacts, all subjected to the same light treatment. Colorimetry measurements confirm a large diversity in the fading behavior, which does not depend on light or other environmental variations (*e.g.* temperature, humidity or anoxia) but is intrinsic to the samples.

XANES spectra at the Fe K-edge for three of these model-artefacts before and after fading further evidence the variability of both PB structures and fading behaviors (Fig. 8). Even before light treatment, PB spectra have different shapes (see pre-edge and post-edge regions), confirming either the influence of the synthesis conditions on the PB structure[46] or, as demonstrated here, the modification of the structure of Prussian blue upon deposition. After fading, a shift of the absorption edge towards lower energies is observed for at least two samples, suggesting a lower average oxidation number of iron atoms, in agreement with the fading process due to the reduction of PB. As well, the extent to which XANES spectra differ after fading seems to be correlated with the amount of color change. For instance, a clearly observable shift of the edge is observed for DDH samples, together with a larger ΔE value (Fig. 8).

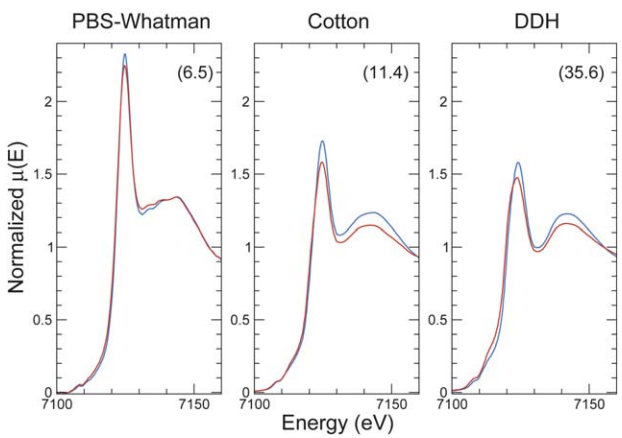

Fig. 8 Normalised XANES spectra of unfaded (blue) and faded (red) Prussian blue artefacts on paper (PBS–*Whatman*), textile (cotton) and gelatin (DDH) samples. ΔE values are indicated in parentheses at the top of each XANES spectrum.

4 Conclusion

In order to further understand the variability of the fading behavior of Prussian blue in cultural artefacts, several factors have been shown to be particularly influential and deserve increased attention.

First of all, the structure of Prussian blue is complex and possesses interrelated features which are likely to influence the final fading behavior of the pigment. In particular, the location of cations within the structure, the water network and the ordering of vacancies determine the availability of the Fe^{II}–C≡N–Fe^{III} units and could play a significant role in the final capacity of the structure to photoreduce. Investigations by XANES and spectrophotometry of PBS–paper samples have shown that the process of PB photoreduction goes beyond a mere reduction of iron(III) and implies complex and correlated changes within the structure, such as significant geometrical distortions of the iron coordination sphere, migration of cations within the structure and/or rearrangement of the water network. The next mandatory steps to further elucidate the interrelationship between PB structure, color and light sensitivity will certainly involve detailed structural interpretation of the XANES spectra, coupled with other analytical techniques such as X-ray diffraction or Mössbauer spectroscopy.

Second, the structure of PBS and its variations are highly dependent on the substrate, which definitely contributes to the various fading behaviors observed. The substrate does indeed play roles at several levels: it can modify the structure of Prussian blue by simple contact (*e.g. Step3* paper), play an active role during its photoreduction (*e.g.* by providing K^+ that catalyze the redox process), or it simply contributes indirectly to the fading process, either by participating in the color change (*e.g.*

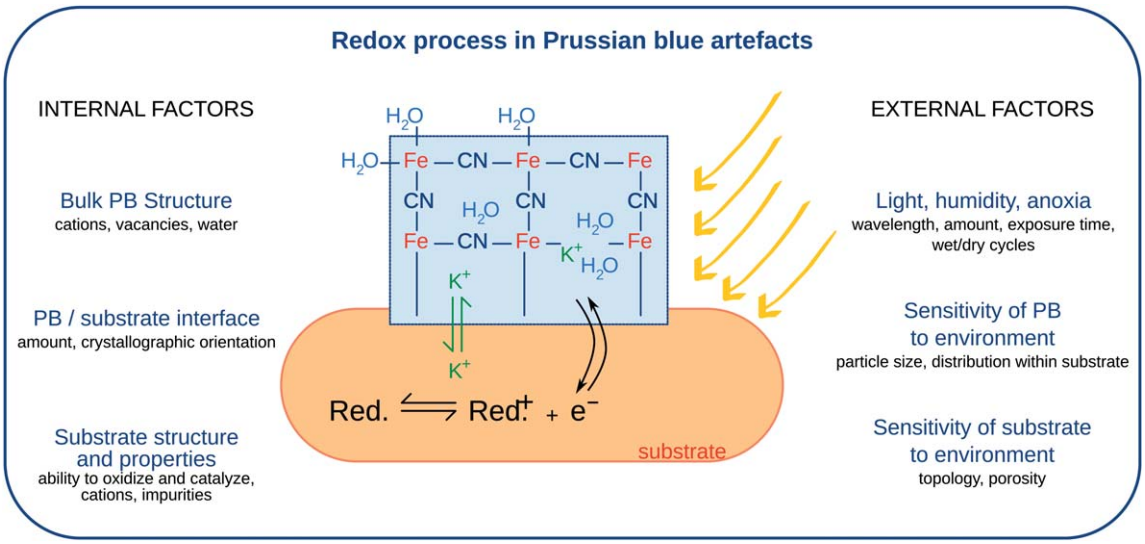

Fig. 9 Summary of internal and external factors playing a role in the redox processes in Prussian blue–substrate systems. In this paper, we have particularly emphasized on the impact of "Bulk PB structure" and "Substrate structure and properties" on the fading behavior of model PB–paper systems. The impact of "Light, humidity, anoxia" was partly investigated on similar PB–paper systems by Gervais *et al.*[18]

yellowing of *Step3* paper) or by influencing the distribution of PB particles and thus their exposure to light. Owing to its various roles, further in-depth investigation of the substrate photodegradation[49,50] in relation to PB photoreduction will certainly help in getting a general picture of the fading mechanism.

As summarized in Fig. 9, the redox properties of PB–substrate systems are influenced by a number of internal and external factors, which are likely to be correlated one with the other. A systematic study of all these features, with a back-and-forth investigation of the entire system at both microscopic and macroscopic levels is required to further understand this complex physico-chemical process generally termed "Prussian blue fading". This approach is here applied to Prussian blue but is also valid for many other cultural heritage materials featuring the trio pigment–substrate–environment. In a broader view, this study, like other recent papers,[19,20] confirms the importance and interest of investigating thoroughly the physico-chemical processes happening in cultural materials and the bias that could be brought by oversimplistic models based on unsupported pigments. In that respect, model samples where history, composition and environmental factors are controlled are invaluable tools to conceptualize these processes. They help in finding the principal causes of degradation and factors which need to be particularly monitored. We hope to demonstrate the interest of developing such an approach based on models, which, coupled with the characterization of real cultural artefacts, could help conservators and restorators in choosing knowingly appropriate conservation treatments on a more rational basis than immediate, visible impacts.

Acknowledgements

We deeply thank K. Chaouchi and S. Blanchandin for their help in preparing the samples, Dr E. Elkaïm for his help on the CRISTAL beamline and Dr P. Dumas for access to the Raman spectrometer. We thank Dr P. Ropret also for the paint samples and M. Ballard for information about Prussian blue dyeing. C. Gervais would like to acknowledge the Swiss National Science Foundation for partial funding of this project through the grant no.138986, as well as Dr T. Wüst and Prof. P. Laszlo for useful comments. We thank Dr R.J. Koestler for suggesting investigation of Prussian blue fading in cultural artefacts. This work has been developed as part of the IPANEMA/Smithsonian Institution agreement on science cooperation.

References

1 B. Lavédrine, C. Pesme, C. Garnier and M. Gillet, Support/Tracé, 2005, **5**, 38–45.
2 S. Rowe, *Stud. Conserv.*, 2004, **49**, 259–270.
3 R. Koestler, E. Parreira, E. Santoro and P. Noble, *Stud. Conserv.*, 1993, **38**, 265–273.
4 M. Ware, *J. Chem. Educ.*, 2008, **85**, 612–620.
5 J. Kirby and D. Saunders, *National Gallery Technical Bulletin*, National Gallery Company Limited, 2004, vol. 25, pp. 73–99.
6 C. Asai, *Zeitschrift für Kunsttechnologie und Konservierung*, 2004, **17**, 261–292.
7 H. J. Buser, D. Schwarzenbach, W. Petter and A. Ludi, *Inorg. Chem.*, 1977, **16**, 2704–2710.
8 F. Herren, P. Fischer, A. Ludi and W. Halg, *Inorg. Chem.*, 1980, **19**, 956–959.
9 J. F. Keggin and F. D. Miles, *Nature*, 1936, **137**, 577–578.
10 K. Nassau, *The Physics and Chemistry of Color: The Fifteen Causes of Color*, John Wiley and Sons, 1983, vol. 1, pp. 147–148.
11 R. J. Mortimer and D. R. Rosseinsky, *J. Chem. Soc., Dalton Trans.*, 1984, **9**, 2059–2061.

12 V. B. Nechitayilo, V. I. Styopkin, Z. A. Tkachenko, Y. G. Goltsov, V. P. Sherstyuk and V. V. Zhilinskaya, *Electrochim. Acta*, 1995, **40**, 2501–2504.

13 K. Itaya, K. Shibayama, H. Akahoshi and S. Toshima, *J. Appl. Phys.*, 1982, **53**, 804–805.

14 A. A. Karyakin, *Electroanalysis*, 2001, **13**, 813–819.

15 J. Agrisuelas, P. R. Bueno, F. F. Ferreira, C. Gabrielli, J. J. Garcia-Jareno, D. Gimenez-Romero, H. Perrot and F. Vicente, *J. Electrochem. Soc.*, 2009, **156**, P74–P80.

16 B. J. Feldman and O. R. Melroy, *J. Electroanal. Chem.*, 1987, **234**, 213–227.

17 M. Ware, *Cyanotype: The History, Science, and Art of Photographic Printing in Prussian Blue*, National Museum of Photography, Film, and Television, Bradford, UK, 1999.

18 C. Gervais, M.-A. Languille, S. Réguer, M. Gillet, S. Chagnot, F. Baudelet, E. P. Vicenzi and L. Bertrand, *Appl. Phys. A: Mater. Sci. Process.*, 2013, **111**(1), 15–22.

19 V. Rouchon, M. Duranton, C. Burgaud, E. Pellizzi, B. Lavedrine, K. Janssens, W. de Nolf, G. Nuyts, F. Vanmeert and K. Hellemans, *Anal. Chem.*, 2011, **83**, 2589–2597.

20 J. Thomas, J. H. Townsend, S. Hackney and M. Strlic, *Polym. Degrad. Stab.*, 2010, **95**, 2343–2349.

21 L. Samain, G. Silversmit, J. Sanyova, B. Vekemans, H. Salomon, B. Gilbert, F. Grandjean, G. J. Long, R. P. Hermann, L. Vincze and D. Strivay, *J. Anal. At. Spectrom.*, 2011, **26**, 930–941.

22 W. Caseri, *J. Mater. Chem.*, 2010, **20**, 5582–5592.

23 L. Matisová-Rychlá, V. Bukovský, J. Rychlý and M. Pleteníková, *Macromol. Symp.*, 2007, **247**, 349.

24 H. Liang, *Appl. Phys. A: Mater. Sci. Process.*, 2011, **106**, 309–323.

25 *The Effects of Air Pollutants on the Accelerated Ageing of Cellulose Containing Materials – Paper*, TNO Report BU 3.94/1068/JH, Delft, The Netherlands technical report, 1994 http://www.viks.sk/chk/res_4_95_209_233.doc.

26 J. Napier, *A Manual of Dyeing and Dyeing Receipts*, Charles Griffin and Co, 3rd edn, 1875.

27 M. Newville, *J. Synchrotron Radiat.*, 2001, **8**, 322–324.

28 E. Reguera, J. Fernandez-Bertran, A. Dago and C. Diaz, *Hyperfine Interact.*, 1992, **73**, 295–308.

29 A. Le Bail, H. Duroy and J. Fourquet, *Mater. Res. Bull.*, 1988, **23**, 447–452.

30 A. C. Larson and R. B. Von Dreele, *General Structure Analysis System (GSAS)*, Los Alamos National Laboratory Report LAUR 86–748 technical report, 2000.

31 K. Hayakawa, K. Hatada, P. D'Angelo, S. Della Longa, C. R. Natoli and M. Benfatto, *J. Am. Chem. Soc.*, 2004, **126**, 15618–15623.

32 G. A. Waychunas, M. J. Apted and G. E. Brown, *Phys. Chem. Miner.*, 1983, **10**, 1–9.

33 T. Westre, P. Kennepohl, J. DeWitt, B. Hedman, K. Hodgson and E. Solomon, *J. Am. Chem. Soc.*, 1997, **119**, 6297–6314.

34 A. Bianconi, M. Dell'Ariccia, P. Durham and J. Pendry, *Phys. Rev. B*, 1982, **26**, 6502–6508.

35 A. L. Dupont, C. Egasse, A. Morin and F. Vasseur, *Carbohydr. Polym.*, 2007, **68**, 1–16.

36 J. C. Wojdel and S. T. Bromley, *J. Phys. Chem. B*, 2006, **110**, 24294–24298.

37 K. Kim, I. Jureviciute and S. Bruckenstein, *Electrochim. Acta*, 2001, **46**, 4133–4140.

38 J. Rychly, L. Matisova-Rychla, V. Bukovsky, M. Pletenikova and M. Vrska, *Macromol. Symp.*, 2006, **231**, 178–192.

39 L. Dupont, J. Bouanda, J. Ghanbaja, J. Dumonceau and M. Aplincourt, *J. Colloid Interface Sci.*, 2004, **279**, 418–424.

40 J. A. Schmidt, C. S. Rye and N. Gurnagul, *Polym. Degrad. Stab.*, 1995, **49**, 291–297.

41 N. R. de Tacconi, K. Rajeshwar and R. O. Lezna, *Chem. Mater.*, 2003, **15**, 3046–3062.

42 D. R. Rosseinsky, J. S. Tonge, J. Berthelot and J. F. Cassidy, *J. Chem. Soc., Faraday Trans. 1*, 1987, **83**, 231–243.

43 H. D. Burgess, in *Historic Textile and Paper Materials*, ed. H. L. Needles and S. H. Zeronian, American Chemical Society, 1986, vol. 212, ch. 20, pp. 363–376.

44 A. Lerwill, J. H. Townsend, H. Liang, J. Thomas and S. Hackney, *e-Preservation Science*, 2008, **5**, 17–28.

45 Y. H. Ngo, D. Li, G. P. Simon and G. Garnier, *Adv. Colloid Interface Sci.*, 2011, **163**, 23–38.

46 S. F. A. Kettle, E. Diana, E. M. C. Marchese, E. Boccaleri and P. L. Stanghellini, *J. Raman Spectrosc.*, 2011, 2006–2014.

47 K. Castro, M. D. Rodriguez-Laso, L. A. Fernandez and J. M. Madariaga, *J. Raman Spectrosc.*, 2002, **33**, 1725.

48 L. Bertrand, M. Thoury and E. Anheim, *J. Cult. Heritage*, 2013, **14**, 277–289.

49 *Ageing and stabilisation of paper*, ed. M. Strlic and J. Kolar, National and University Library, Ljubljana, Slovenia, 2005.

50 M. Manso and M. Carvalho, *Spectrochim. Acta, Part B*, 2009, **64**, 482–490.